INFLUENCE OF BURIED INTERFACES ON THE CHARGE

DYNAMICS IN OXIDE THIN FILMS

by

Shreedhar Nath Pant

Master in Physics, 2006
Tribhuvan University
Kathmandu, Nepal

Submitted to the Graduate Faculty of the
College of Science and Engineering
Texas Christian University
in partial fulfillment of the requirements
for the degree of

Master in Science

August 2015

Acknowledgements

I would like to deeply thank my advisor Dr. Yuri Strzhemechny for his guidance and patience. He has been very helpful in my research.

I would like to thank my lab partners, fellow graduate students and faculty members for their valuable suggestions.

I would also like to thank Professor Jeffery Coffer from TCU Chemistry Department for kindly allowing to use the Raman spectroscopy equipment, his graduate students for their help with running the Raman experiments and Professor Andrey Chabanov (University of Texas at San Antonio) and his group for the thin film ZnO samples provided for our studies.

Table of contents

VITA

Abstract

List of figures

List of acronyms

Acronyms	Definitions
AFM	Atomic force microscopy
ALD	Atomic layer deposition
CPD	Contact potential difference
E_c	Conduction band
E_F	Fermi level
E_g	Bandgap
E_t	Surface state
E_v	Conduction band
LT	Low temperature
Q_{sc}	Net charge in the SCR
Q_{ss}	Net surface charge
QTH	Quartz tungsten halogen
RT	Room temperature
SCR	Surface space charge region
SPV	Surface photovoltage
TiO_2	Titanium dioxide
UV	Ultraviolet
V_s	Surface potential
ZnO	Zinc oxide

Introduction

Oxide semiconductors have been attracting considerable attention across many fundamental and applied fields of study. These materials exhibit diverse structural, electronic and optical properties. Their potential applications range from optoelectronic devices, energy generation, and storage, biotechnology, and for many of these applications, thin films are the structures of choice [1].

The surface of a thin film is oftentimes essential for determining the properties of the entire system. At the free surface of a semiconductor, the periodic structure is terminated, which leads to the formation of defects that induce electronic states within the bandgap. Importantly, adsorption or desorption of foreign species from the environment could modify these states [2]. In addition to the defects at the free surface, in the thin film structure an important role could be played by defect states at the interface with the substrate. These interface states may, in turn, influence surface properties of the thin film system. Thus, it is appealing to elucidate the role of buried interfaces, i.e. located more than few nanometers below the free surface, in key performance domains of such thin-film systems. In this work, we investigate the role of buried interfaces as well as the influence of environments on the surface optoelectronic properties in thin films containing ZnO.

ZnO has been studied and employed for such applications as solar cell [3], light emitting diodes [4-6], photodetectors [7],. It is well known that the interface defects can act as charge recombination centers degrading performance of ZnO thin film devices [3]. The quality of the ZnO layer depends on the synthesis methods and growth parameters such as temperature [3-7]. Thus, influence of growth temperatures on the electronic structure at the

1

buried interface of a ZnO thin film is of great interest. In our work, we investigated ZnO thin films grown by atomic layer deposition (ALD) on Si substrates at different temperatures, addressing a question of how the variation of the ALD growth temperature affects the electronic structure at the buried interface with the substrate.

The photoresponse behavior of ZnO thin films, despite the sizable body of research, is still rather poorly understood. It has been observed that, remarkably, the photoresponse would not saturate for hours or days after the illumination was switched off [2, 7-8]. The origin of this effect has been debated extensively with some authors attributing it to the slow trapping of the photoexcited electrons at the surface defects whereas others assign it to the presence of the metastable conductive states related to bulk defects, such as oxygen vacancy [2,7-8]. Adequate understanding of the origin of photoresponse is necessary to control the performance of, ZnO-based photovoltaic devices. Here, by investigating the photoresponse of ZnO thin films ALD-grown at various temperatures we develop a model for the observed behavior based on the adsorption and desorption of species present at the surface of ZnO under different environmental conditions.

In our study we use surface photovoltage (SPV) and photoluminescence (PL) both of which are non-destructive experimental techniques probing optoelectronic characteristics of materials to investigate the influence of the buried interfaces on the charge dynamics and how the buried interfaces and ambient conditions affect the photoresponse properties after turning off illumination in oxide thin films. They can be operated in different ambients and SPV, in particular, is sensitive to buried interfaces.

Zinc oxide (ZnO)

ZnO is a compound semiconductor formed by group II element Zn and group VI element O with a wide direct bandgap of ~ 3.3 eV at 300 K with a high exciton binding energy of 60 meV [9]. At ambient conditions ZnO crystallizes in a hexagonal wurzite structure with a mixed ionic/covalent bonding. The valance band is formed by the oxygen $2p$ states while the conduction band – by the Zn $4s$ states. In a lattice each Zn ion is surrounded by four O ions [9].

Undoped ZnO exhibt an n-type conductivity, most likely due to oxygen vacancies and zinc interstitials [9]. However, according to the Van de Walle hydrogen can act as shallow donor [10]. Thus, the source of the n-type conductivity is still unclear. For the successful device applications employing homojunctions, it is necessary to have a p-type ZnO. At present reproducible growth of a p-type ZnO remains challenging primarily because the source of the n-type conductivity is still unclear, thus in device applications ZnO heterostructures are used, most of the time on such substrates as Si, GaN, sapphire, etc [2-7].

Among others, Si has been extensively used as a substrate for ZnO thin films because of the low cost, large wafer sizes and commercial availability [4]. The most common applications of ZnO thin film on Si are in light emitting diodes and photodetectors [2- 8]. The interface between ZnO and Si is the major source of defects due to the large lattice mismatch. These interface defects can act as charge recombination centers degrading the efficiency of the ZnO/Si devices, thus the control of the defect concentration at the ZnO/Si interface is highly desirable.

On the other hand electronic, structural and optical properties of such ZnO/Si systems depend on the growth method [11-13]. Various methods have been used for the production of ZnO thin films such as metal-organic chemical vapor deposition [6], pulsed-laser deposition [2], and atomic layer deposition (ALD) [11-13]. In recent years ALD has been increasingly utilized to grow ZnO thin films suitable for device applications. Advantages of ALD over the other methods are the ease and accuracy of thickness control, conformal step coverage, high uniformity over large areas, low defect density, low deposition temperatures, and good reproducibility [11-13]. Characteristics of ALD-grown ZnO depend on the growth parameters. For example, the structural and optoelectronic properties of ALD-grown ZnO were investigated in [11-13] as a function of the purging and pulsing time, and it was found that the optical emission depends strongly on the purging time. Reportedly, the OH groups are abundant in the samples with low purging time and they act as non-radiative recombination centers [12]. In [11] the authors investigated ZnO thin films ALD-grown on sapphire substrates at temperatures in the 150°C-350°C range employing PL. PL of ZnO typically shows emission in two spectral regions – UV, corresponding to the near-band edge transitions (e.g. exciton recombination), and visible, corresponding to the defect-related deeper levels (e.g., oxygen vacancies or zinc interstitials) [11-13]. A weaker defect level emission indicate the higher crystalline of ZnO thin film. In [11] the sample grown at 200°C showed intense near-band edge and negligible deep defect level intensity. Thus, the enhanced near-band edge and suppressed deep defect level emission indicate the sample grown at 200°C is of higher crystalline quality. On the other hand, E Przezdziecka et al., studied ZnO ALD-grown on Si at 100°C, 130°C, and 200°C and found that ZnO with the highest quality can be obtained at 130°C [13].

Thus, the ALD technique allows growth of ZnO thin films in a rather wide range of relatively low temperatures, which, in turn, strongly affect the optoelectronic properties of ZnO. These factors motivate us to explore the electronic structure of the buried interfaces of ZnO thin films grown on Si by ALD. In particular, we address the question of how the ALD growth temperatures affect this electronic structure. To the best of our knowledge, the effect of the growth temperatures on the electronic structure of buried interfaces has not been studied in ALD grown ZnO. In our work employing PL and SPV we investigate ZnO thin films ALD-grown on Si substrates at four different temperatures – 120°C, 150°C, 170°C, and 200°C.

The surface of ZnO, like in many other semiconductors, is sensitive to the environment. The adsorbed impurities and gas species from the environment may create new or modify existing gap states [2]. Under illumination these species on the surface may exchange charge with ZnO which also could significantly change the surface band bending and thus affect the charge transport properties of the semiconductor. In the SPV studies of ZnO reported to date, effects of environment were addressed in a relatively small number of papers [14-15]. For example, for ZnO nanorod arrays discussed in [14] it was observed that their SPV response disappears in vacuum and reappears again in the oxygen environment. Transient SPV curves of ZnO thin films investigated in [8] did not saturate for hours/days after switching off the illumination, which was attributed to energy levels with different lifetimes in the ZnO thin films. Nevertheless, the number of reports on the subject remains very limited, with many issues such as influence of buried interfaces remaining elusive. Thus, in our studies we address the question of how different experimental environmental conditions could affect the charge dynamics in the studied ZnO thin films. To answer this

question it is important to investigate persistent photoconductivity and photovoltage features in the samples of interest.

Experimental method

Experimental probe sensitive to the buried interfaces are necessary to investigate the role of buried interfaces on oxide thin films grown on semiconductors substrates. We performed analysis of ZnO thin films grown on *n*-type Si employing surface photovoltage spectroscopy (SPV) and photoluminescence (PL).

Surface photovoltage (SPV)

Surface photovoltage (SPV) is a contactless experimental technique for characterization of a semiconductor surface and the subsurface vicinity. SPV measures the change in the surface potential upon illumination. It can provide information on, among others, surface band bending, surface charge, surface dipole, as well as surface and bulk charge recombination rates, conductivity type, energetics of surface and bulk states.

Atoms in crystals are periodically arranged. At the free surface, the periodic structure is terminated, giving rise to electronic states which in the case of a semiconductor crystal are surface-localized within the bandgap. These surface-localized states may induce charge transfer between the bulk and the surface to establish thermal equilibrium between the two. This charge transfer results in electrically non-neutral near surface-region referred to as the surface space charge region (SCR) [16]. Therefore, the surface potential (V_s) is different from the electrical potential far away in the bulk even under the equilibrium condition. This means that the semiconductor bands are bent in the vicinity of the surface. For example, the

upward band bending in an *n*-type semiconductor is shown in figure 1(where E_c is the conduction band, E_v is the valence band, E_g is the band gap, E_t is the surface state) is due to the negative charge transfer from the bulk to the surface states.
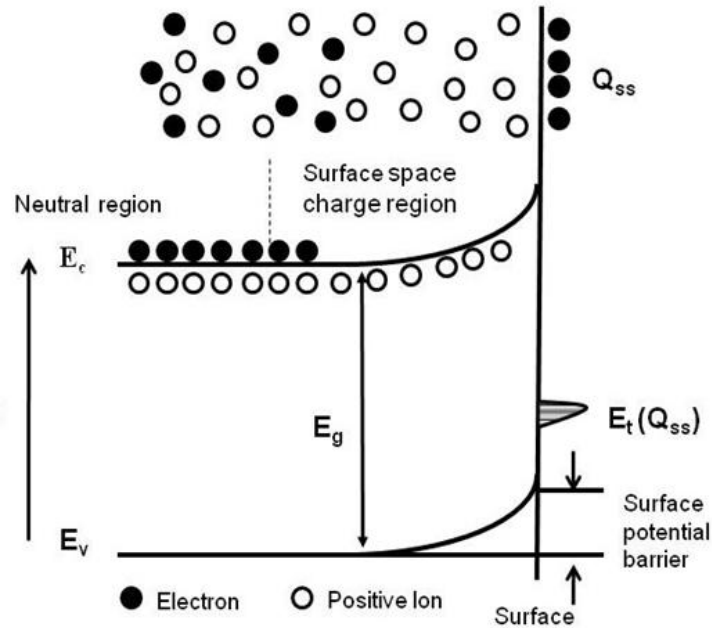
Figure 1: Effect of surface states on the near-surface charge redistribution of in an n-type semiconductor [17].

In SPV experiment one measures the value of V_s. It is dictated by the charge conservation rule:

$$Q_{ss} = -Q_{sc}, \qquad (1)$$

where Q_{ss} is the net surface charge and Q_{sc} is net charge in the SCR.

There are two primary charge transport mechanisms responsible for the generation of the SPV signal: diffusion and drift. When a semiconductor surface is illuminated with

photons of certain energy, this induces formation of free carriers (electron-hole pairs) via band-to-band transitions and/or release (capture) of the carriers at the surface states via trap-to-band (band-to-trap) transitions. These processes change the near-surface concentration of electrons and holes compared to the bulk of the material. The concentration gradient of free charge carriers is established along with an induced electric field leading to excess charge accumulation at the surface as a result of diffusion/drift. This, in turn, leads to the change in the height of the surface potential barrier and generates the SPV response.

Generally, SPV depends strongly on whether the incident photon energy is super-bandgap or sub-bandgap. In a super-bandgap SPV, when a semiconductor absorbs photons with the energy greater than the bandgap E_g, electron-hole pairs are generated by the transition of electrons from the valance band to the conduction band. In this case, trap-to-band transitions can be mostly neglected [16]. For example, considering an n-type semiconductor, as shown in figure 2, illumination with super-bandgap photons excites the electrons from the valance band to the conduction band, the electrons move toward the bulk whereas the holes − toward surface due to the electric field. This mechanism reduces the density of the surface-trapped electrons (i.e., the surface acquires more positive charge) and the band bending is reduced. Conversely, in the second super-bandgap mechanism, as shown in figure 3, either electrons or holes are preferentially trapped by the surface states. This also changes the surface potential.
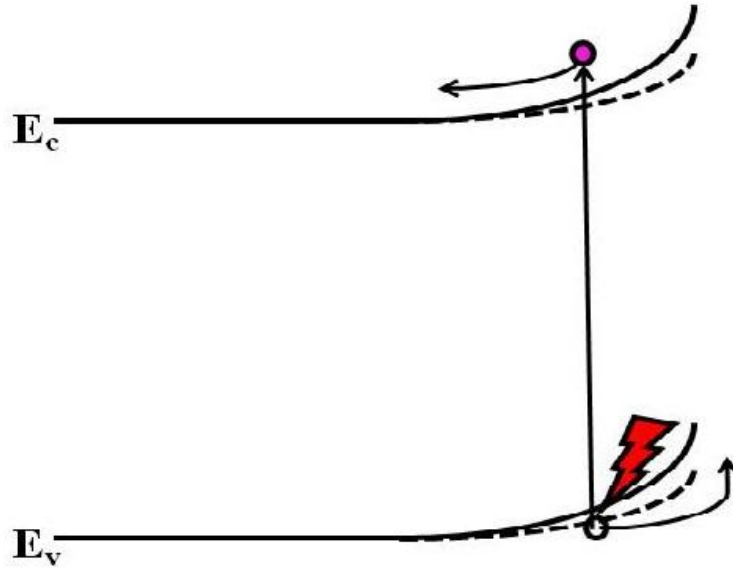
Figure 2: Super- bandgap illumination with carrier separation under the influence of an electric field. Solid and dashed lines represent band positions in dark and under illumination correspondingly [18].
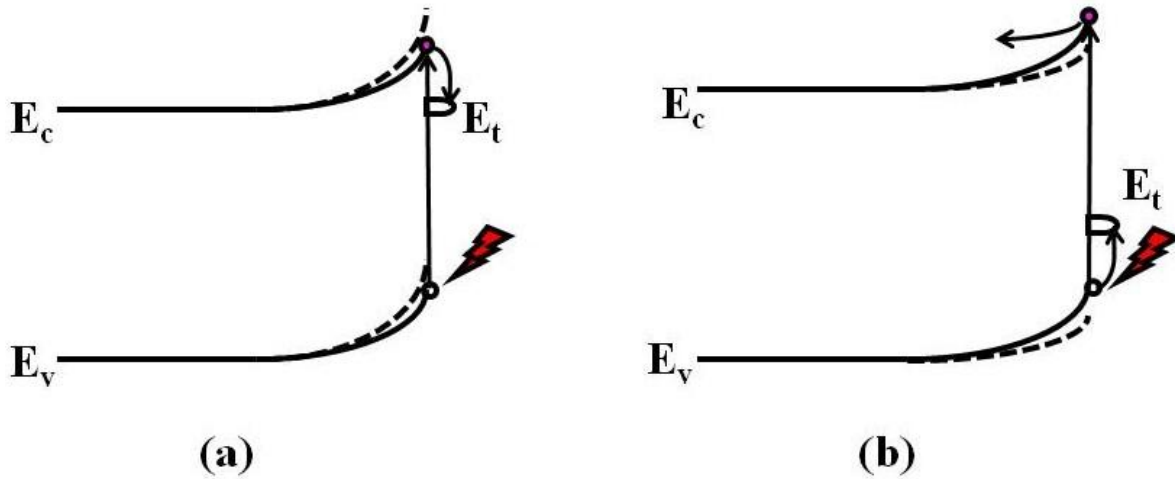
Figure 3: Super-bandgap SPV with preferential trapping of (a) electrons, (b) holes. Solid and dashed lines represent band positions in dark and under illumination correspondingly [18].

A sub-bandgap SPV transition takes place if a semiconductor absorbs photons with energy smaller than E_g. In the case of an *n*-type semiconductor, with a surface state E_t, illumination with photons of energy higher than the energy difference between the bottom of the conduction band E_c and the surface state E_t promotes electrons transitions from the surface state into the conduction band. The excited electrons are quickly swept to the semiconductor bulk under the built-in electric field in the SCR. This is accompanied by a decrease in the band bending as shown in the figure 4(a). This trap-to-band transition is also called the surface state depopulation. Illumination with photons of energy higher than the energy difference between the surface state E_t and the top of the valance band E_v may promote electron transitions from E_v into the surface state which is equivalent to a hole transition from the surface state to the valence band. This transition only takes place if the surface states are not filled before the illumination. Such transition makes the surface more negatively charged and is accompanied by an increase in the band bending, as shown in figure 4 (b).
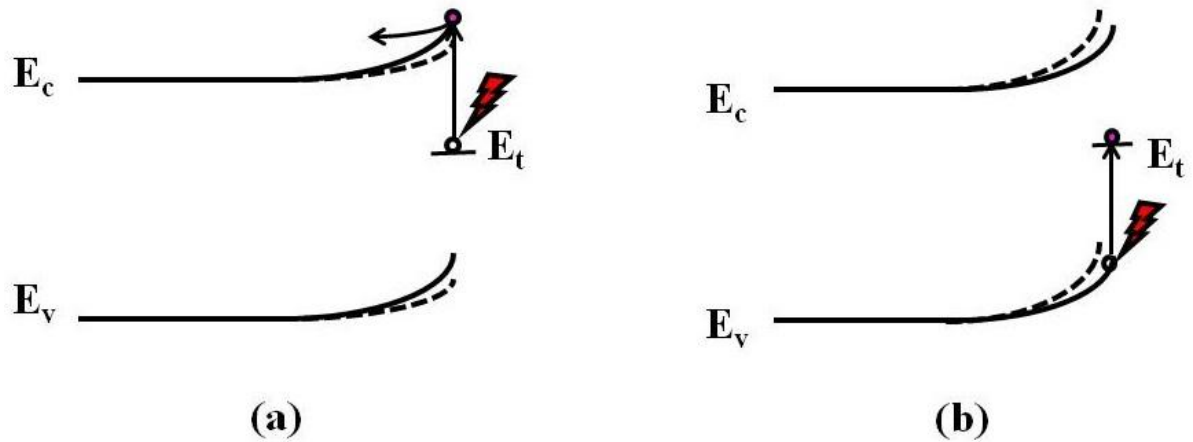
Figure 4: Sub-bandgap illumination with excitation of trapped electrons (a) and holes (b). Solid and dashed lines represent band positions in dark and under illumination correspondingly [18].

Sensitivity of SPV to the buried interface

Optoelectronic properties of oxide thin films could be strongly affected by defects, both intrinsic and extrinsic. Defects may degrade device performance or be beneficial for many applications. For example, in TiO_2 defect-related states within the bandgap can absorb in the visible range, which could be beneficial for sunlight-induced PC activity [19]. The most common intrinsic defects in such semiconductors as ZnO and TiO_2 are the oxygen vacancies.

For the various applications of oxide thin films high quality material that has fewer defects are required and the crucial role is oftentimes played by the interface. The latter could be the major source of defects due to the lattice mismatch. Interface states associated with these defects may give rise to non-radiative recombination centers which may in turn affect charge transport and optical properties. For example, interface states may change the generation/recombination current in *p-n* junctions and modify the depletion region width.

11

The quality of the surface and the interface of thin films depend on the growth methods and growth parameters. Thus, the evaluation of the electronic states at the buried interface is one of the most pressing issues in the devices physics. However, it is quite difficult to investigate the electronic structure at the buried interfaces by most of the surface-sensitive probes. Usually analysis of the buried interfaces using surface techniques requires intrusive sample preparation procedures which may result in a loss of information about the interface. To overcome this difficulty in our studies we employ the non-destructive SPV method that is sensitive to the electronic states in the buried interfaces.

In the previous section, we have discussed the sensitivity of the SPV to the free surface, yet it is important to point out that SPV could be quite sensitive to the buried interfaces as well. In a semiconductor thin film structure there are SCR regions that might form at both the free surface and the interface between the thin film and the substrate. In such cases, the SPV signal would have contributions from both the SCRs illuminated by light, provided the top layer is transparent at least for some wavelengths.
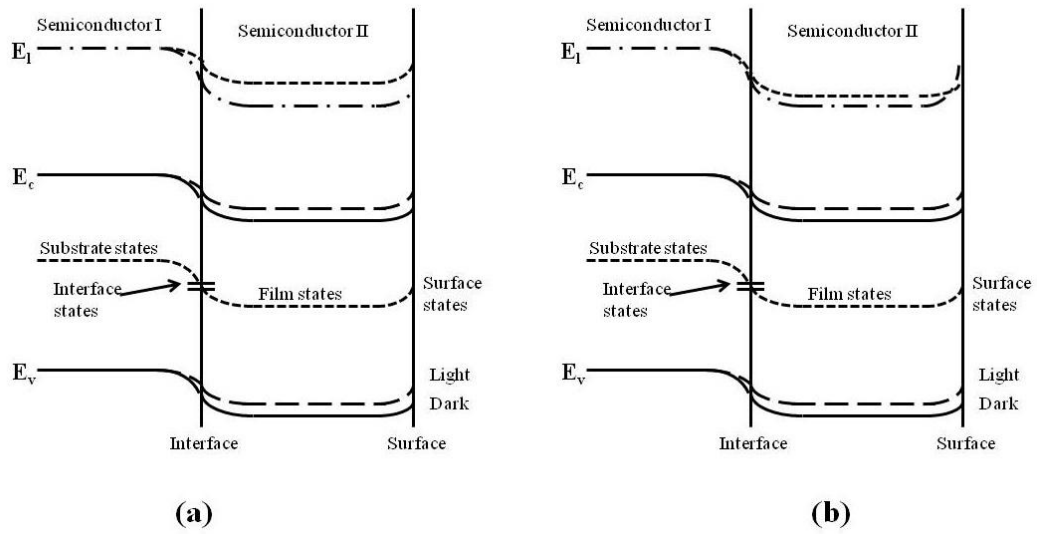
Figure 5: Band-lineup of a typical thin film structure in dark (solid curve) and under illumination (dashed curve), where the dominating contribution to the SPV is from the: (a) interface SCR, (b) surface SCR. [16, 18].

The relative contributions to the SPV signal from the free surface and the buried interface can be understood from the band diagram show in figure 5 [16,18]. Relative contributions to SPV of the surface and the interface can be understood better by introducing the local vacuum level E_l, defined as the energy of an electron at a given point if it is at rest and free from the influence of the crystal potential. One can see that during the light-on event the change of the band bending at the interface region is greater in figure 5(a) than in figure 5(b). Thus, figure 5(a) represents the situation with a dominating contribution to SPV of the interface whereas the figure 5(b) – a dominating contribution from the free surface.

Experimentally various group have confirmed that the SPV is sensitive to the buried interface [20-21]. For example, D Gal et al., in a CdS/CuIn$_x$Ga$_{1-x}$Se$_2$/ZnO structure were able

to identify the bandgaps of all the materials [20]. They also observed that the bandgap of $CuIn_xGa_{1-x}Se_2$ increases as the annealing temperature is increased, which was attributed to the passivation of the defects at the interfaces acting as recombination centers.

The sensitivity of SPV to the buried interface may also lead to the reversal of the spectral line shapes. This has been observed by C. H. Chan et al., while studying the temperature-dependent SPV of $In_xGa_{1-x}As/GaAs$ samples [21]. This kind of reversal in heterostructures can be also understood by the band diagram shown in figure 5. For example, the *n*-type thin film has two SCRs at both the surface and the interface. Decrease in the band bending at the surface will results in a positive SPV whereas decrease in the band bending at the interface will results in a negative SPV [16,18]. Thus the dominating contribution will determine the spectral shape of the SPV, which, as discussed later in this paper, could be observed in the materials studied by us.

SPV measurement

In our SPV experiment we employed the Kelvin probe method to measure changes in the surface potential.

Kelvin probe is a non-contact, non-destructive method to measure the work function difference between two materials which are close to each other forming a parallel plate capacitor. This can be demonstrated by two metals with the work function W_1 and W_2 as shown in the figure 6. Two metals are electrically neutral before connecting (figure 6(a)). Both metals share the same vacuum level. Upon connecting the two metals with a wire (figure 6(a)), charge flows from the metal with the smaller work function to the metal with the larger work function to equilibrate the Fermi levels. This charge flow results in an

electric field and hence a potential difference is set up between the plates. This potential is known as the contact potential difference (CPD). Thus, $eV_{cpd}=W_1-W_2$. The reason for measuring the work function difference is that the surface potential and the work function are dependent. Any change in the surface potential is equal to the change in the work function [18].
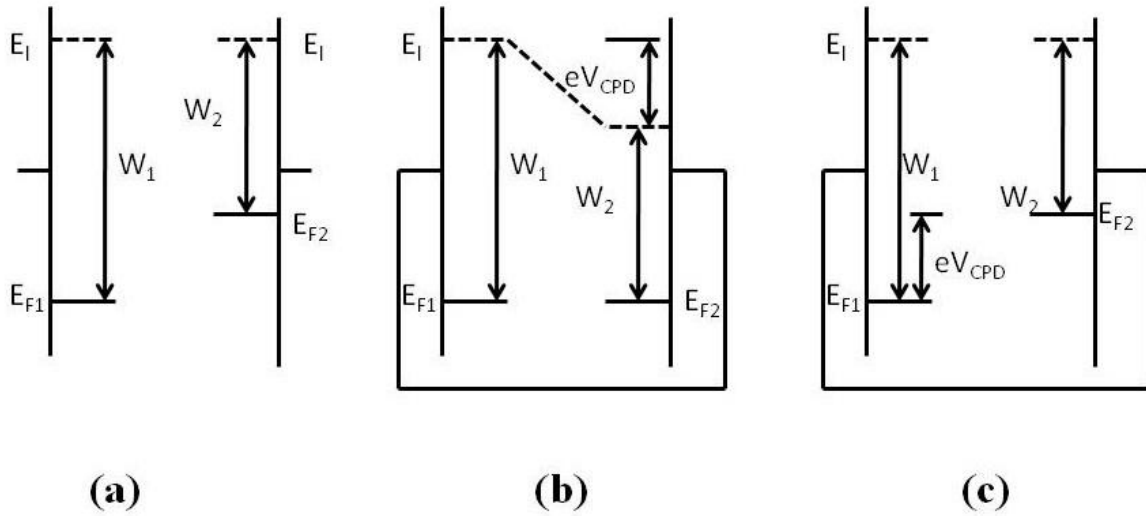
Figure 6: Band diagram of parallel plate capacitor formed from two metal plates: (a) isolated, (b) short-circuited, (c) connected through DC bias equal and opposite to CPD [18].

CPD is measured by the null method proposed by Lord Kelvin. According to this method an external DC bias is applied ((figure 6(c))) which is equal and opposite to CPD and V_{CPD} is measured as the difference of the Fermi level. The Kelvin probe used in our experiments is vibrating close to the sample, thus generating the AC current. An external bias is applied such that the AC current is zero. The value of such bias is equal to the CPD. This value of external bias is determined by the electronics used in the experiment.

SPV experimental setup

Our SPV experimental set up can operate in ultra high vacuum (UHV) or in a gas ambient. The experimental setup sample consists of vibrating Besocke Kelvin probe which is a circular mesh electrode ~2mm in diameter. Kelvin probe is in the fixed position inside the chamber whereas the position of the sample is adjusted by the XYZ manipulator. In order to record the transient response the sample is illuminated with a 30W halogen lamp light which is passed through the optical fiber (with a transmission in the 160-1200 nm range) into the chamber until the saturation is achieved. Then the experiment is continued in the dark. The LabView program records the change in CPD as a function of time. For the duration of the experiment under UHV conditions the turbo mechanical pump and the rotary pump are turned off while the ion pump maintains the vacuum in the system.

In order to collect SPV spectra a 250W QTH (Quartz tungsten halogen) lamp is used as the light source. The light is passed through a pair of fused silica lenses into an Oriel Cornerstone grating monochromator. There are two gratings with wavelength ranges of 180 nm-750 nm and 450 nm-200 nm. Different filters are placed between the light source and the monochromator to eliminate higher order diffraction in the spectra. The illumination is chopped with the mechanical chopper. Optical fiber having transmission range of 160 nm-1200 nm is used to pass the light into the sample inside the chamber. LabView program varies the wavelength range, their interval and the time constant of the SPV spectra. The SPV experiments are performed in complete darkness.

Photoluminescence (PL)

The second defect-sensitive, contactless, nondestructive method used in our work is photoluminescence (PL) spectroscopy. PL is the process in which the material emits radiation after absorption of light. The principle of photoluminescence is illustrated by figure 7 below.

When the sample is excited with the energy of light greater than the bandgap, electrons from the top of the valance band are excited to the conduction band leaving holes in the valance band. The electrons thermalized to the bottom of the conduction band may participate in recombination processes with the holes in the valance band accompanied by the emission of photons with energy equal to the band gap value. Alternatively, the electrons can recombine through the states present within the bandgap, as shown in the figure 7, so that the resulting photons will have energy smaller than that of the bandgap.
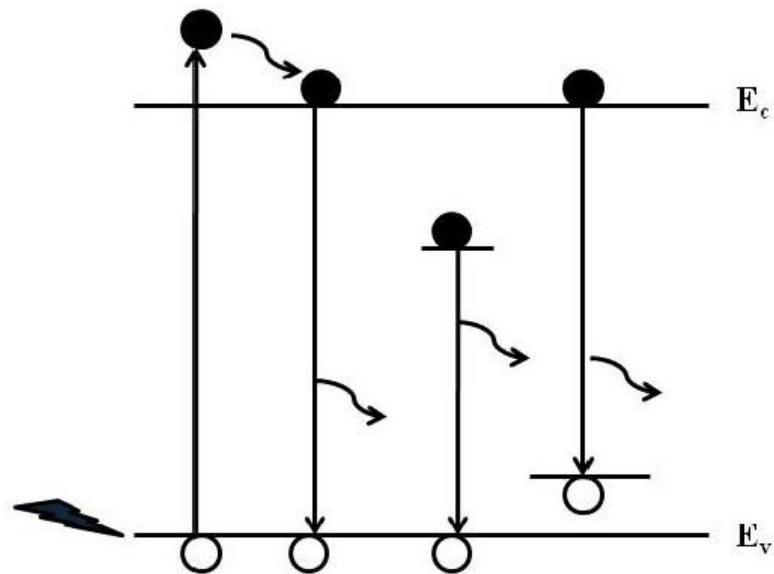
Figure 7: Diagram illustrating process occurring during photoluminescence.

PL setup

The PL setup used in our experiments consists of the excitation light source, light collecting lenses, monochromator and detector. To excite luminescence, we use a continuous-wave HeCd Kimmon laser (model IK5452R-E) operating at 325 nm. The laser beam is focused onto the sample, which is mounted on a sample-holder designed for the Janis CCS-150 closed-cycle helium gas cryostat used to control the temperature of the sample in the 8 K-300 K range. The cryostat is evacuated below 10 mTorr using a mechanical pump before cooling. The luminescence is guided by two lenses into an adjustable entrance slit of a SPEX 1401 double-grating monochromator with a spectral resolution of 0.18 cm^{-1}, an optical path of ~ 4 meters and an F# of 7.8. A photomultiplier tube (PMT) PR C31034 detector is attached to the exit slit of the spectrometer. The PMT output is connected to a Stanford Research lock-in amplifier to subtract the background noise and to convert the current signal into the DC voltage, which is then supplied into a PC through a National Instruments GPIB card.

Atomic force microscopy (AFM)

In a typical AFM setup, a sharp probe tip is attached to a cantilever which is scanned across the sample. The deflection of this cantilever (which is monitored using a laser and a photodiode) is caused by the forces between the tip and the sample. AFM allows imaging of the surface with a nanometer resolution. We have used AFM to measure the surface roughness of the ZnO samples grown on the Si substrate using a nano SOLVER NT-MDT AFM instrument operating in the tapping mode.

Results and discussions

ZnO thin film samples

ZnO thin films were grown on Si (111) wafers using a Savannah 200 ALD instrument (Cambridge NanoTech) at the University of Texas at San Antonio in Professor Andrey Chabanov's laboratory. The films were grown at four different temperatures: 120°C, 150°C, 170°C and 200°C to a thickness of ~ 100 nm.

AFM results

AFM was employed to measure the surface roughness of the samples. Roughness gives us an idea how smooth the surface at a certain length scale. A number of parameters are used to determine the roughness of surfaces.

Average roughness (R_a) is the arithmetic mean of the absolute values of height of the profile Z(x). The roughness average (R_a) is defined as

$$R_a = \frac{1}{L}\int_0^L |Z(x)|dx \qquad (2)$$

Where Z(x) is the function that describes the surface profile analyzed in term of height (Z) and position (x) of the sample over the evaluation length "L" (figure 8).

Ra, is the arithmetic average height of roughness-component irregularities (peak heights and valleys) from the mean line, measured within the sampling length, L. See figure (8).

Root mean square (RMS) roughness (R_q) is the mean squared absolute values of surface roughness profile. Mathematically it is defined as

19

$$R_a = \frac{1}{L}\int_0^L |Z^2(x)|\, dx \qquad (3)$$
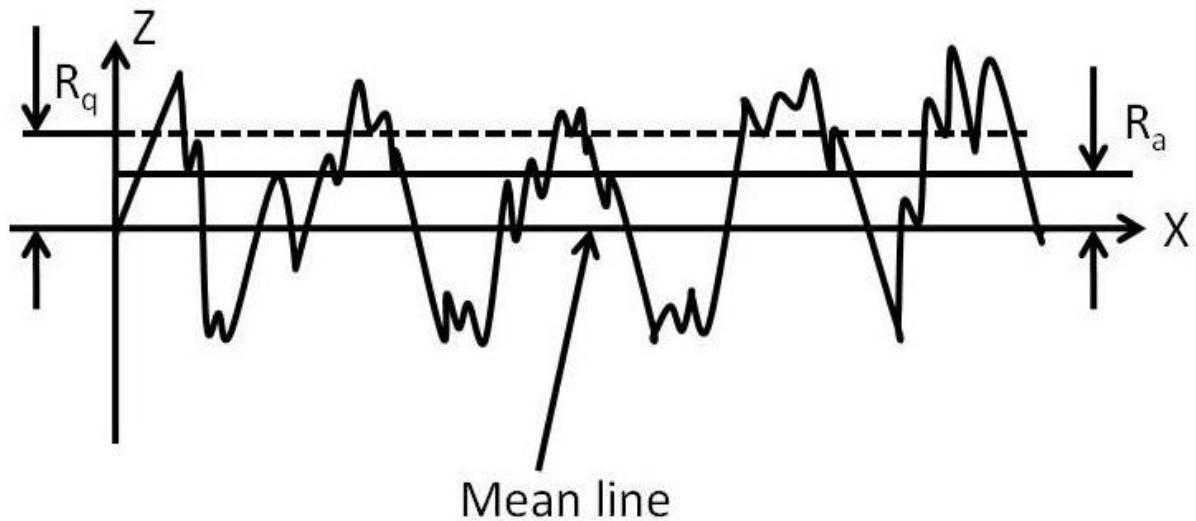
Figure 8: Profile of a surface (Z). It represents the average roughness Ra and Rq is the RMS roughness based on the mean line.

The AFM images are presented in figures 9-12. The RMS roughness is 4.54 nm, 2.79 nm, 1.897 nm and 1.567 nm for the samples grown at 120°C, 150°C, 170°C, and 200°C, respectively. Thereby, there is an obvious trend of decreasing surface roughness with the increase of the growth temperature shown in figure 13.

Figure 9: AFM profile of the ZnO thin film grown at 120°C.

Figure 10: AFM profile of the ZnO thin film grown at 150°C.

Figure 11: AFM profile of the ZnO thin film grown at 170°C.
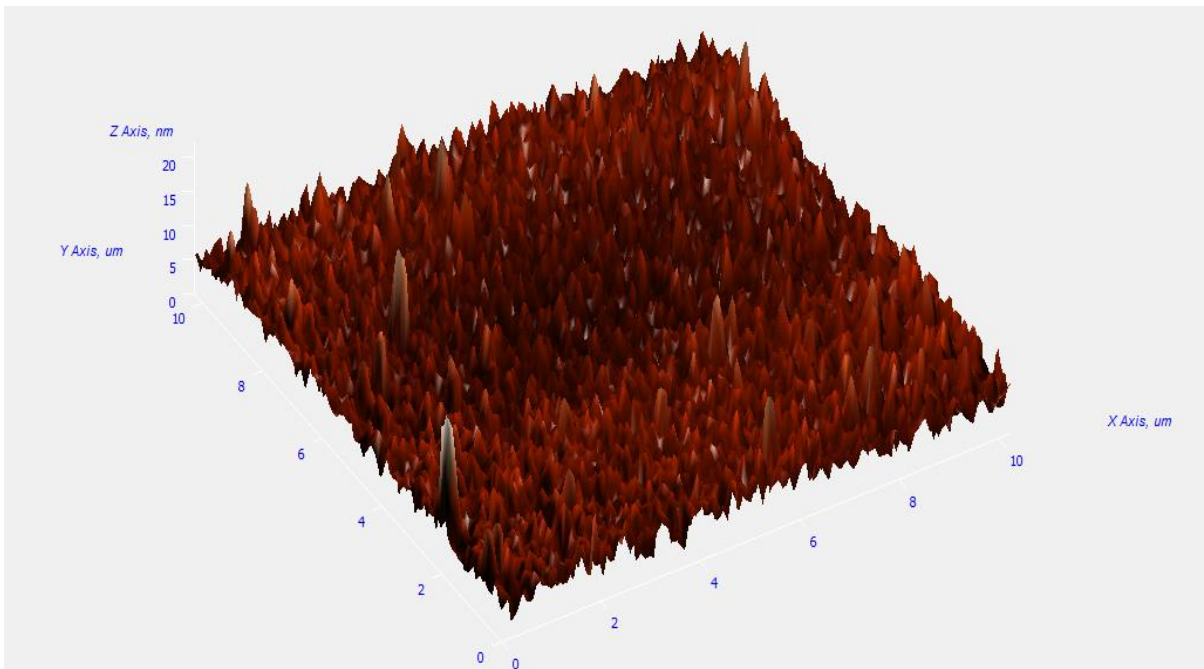
Figure 12: AFM profile of the ZnO thin film grown at 200°C.
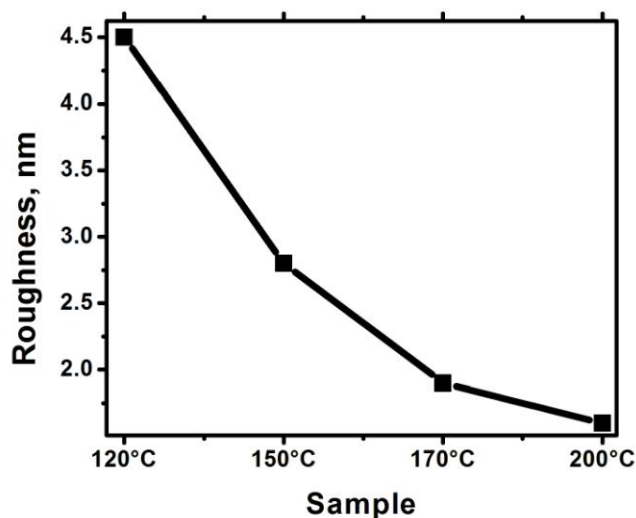
Figure 13: Plot of RMS roughness Vs sample growth temperature.

PL results

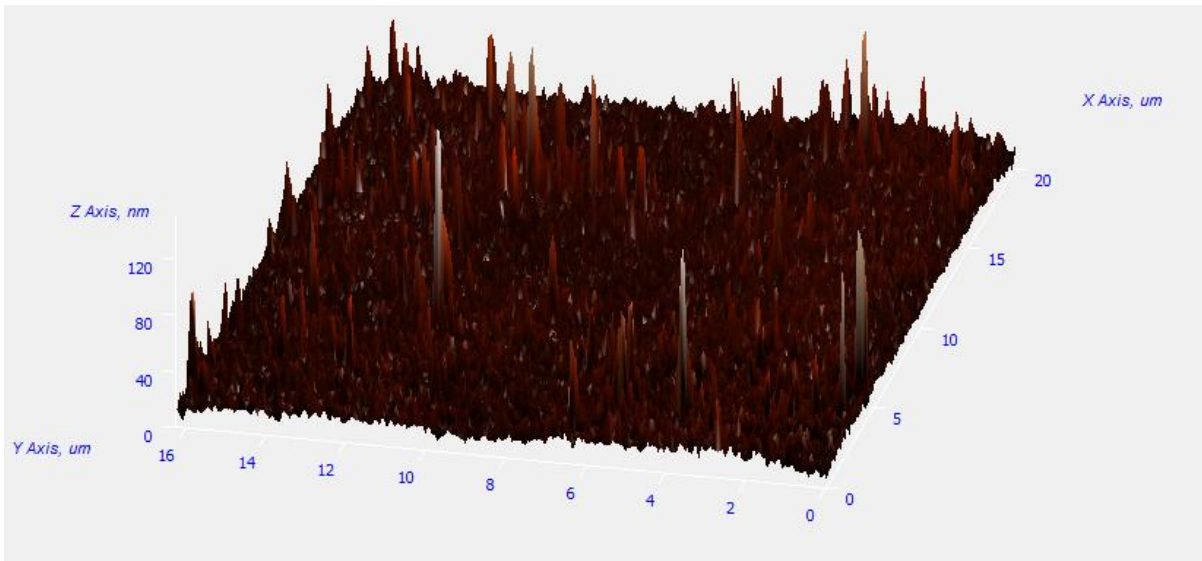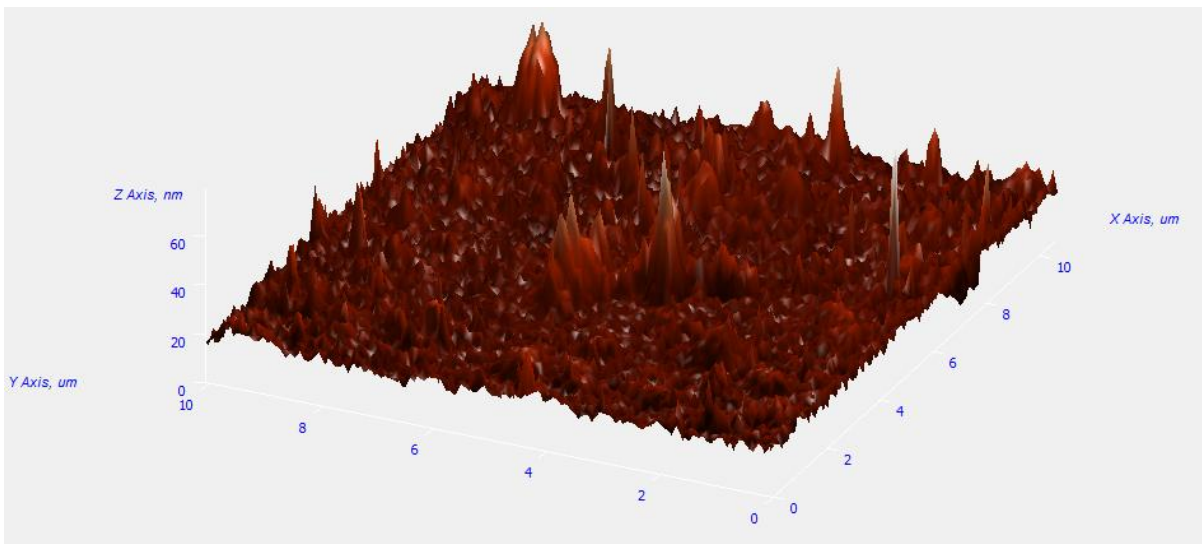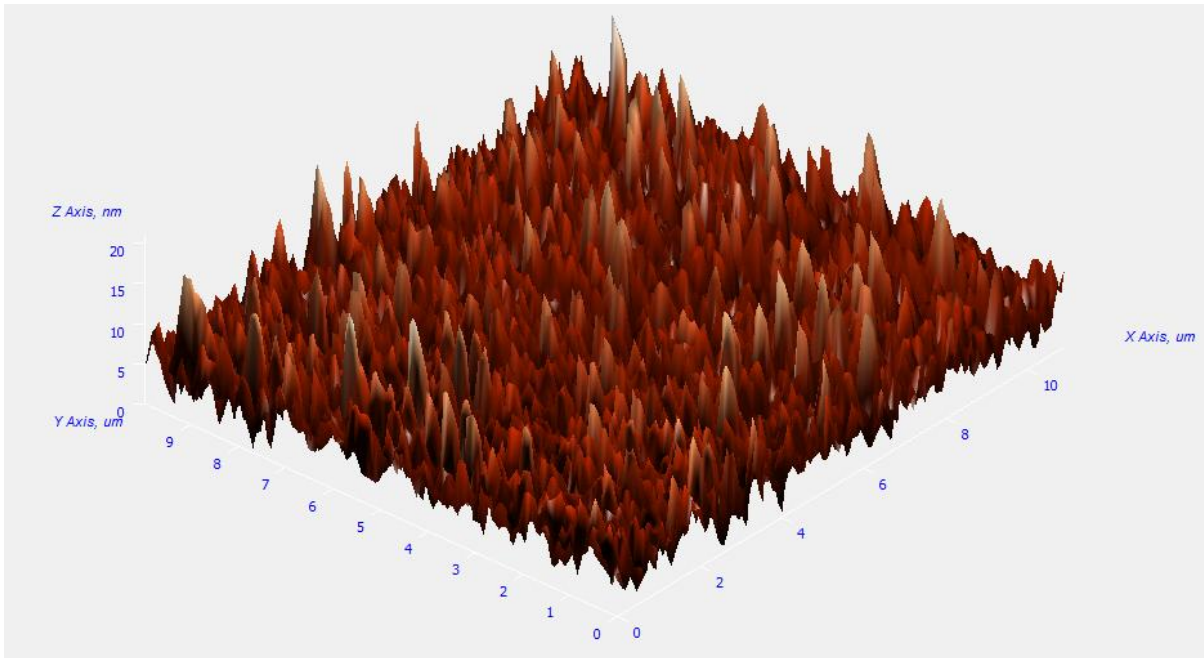PL measurements were preformed in all the samples to measure the optical quality of the thin films grown on Si substrates. We performed PL measurements at room temperature (RT) as well as at the low temperature (LT) of ~ 8 K. These PL spectra are shown in figures 14 and 15. ZnO typically shows emission in two spectral regions – UV, corresponding to the near-band edge transitions (e.g. exciton recombination), and visible, corresponding to the defect-related deeper levels (e.g., oxygen vacancies or zinc interstitials). In the spectra for all the samples studied here, in addition to the UV excitonic emission at ~ 3.3 eV, one can see a violet spectral feature at ~3.1 eV, corresponding to shallow defect transitions. In the RT PL spectra one can see that the relative intensity of the near-band gap luminescence for the sample grown at 120°C is much lower compared to the other samples, whereas the relative intensity of the visible luminescence band related to deep defects is more intense and red-shifted. This is a clear indication of the lower quality (which has higher defect states

23

emission intensity compared to the other samples) of the sample, probably due to an incomplete reaction between the precursors used [11]. At the higher temperatures, the reaction between the precursors is more complete leading to the higher intensity of the UV/violet peaks and reduction of the deep-defect luminescence. The trend of increasing relative intensity of the UV/violet emission and decreasing intensity of the deep-defect luminescence with the growth temperature is even more pronounced in the LT PL spectra. This confirms the importance of the ALD growth temperature on the quality of the obtained material. Moreover, the effect of growth temperature on sample quality is confirmed by our AFM measurements.
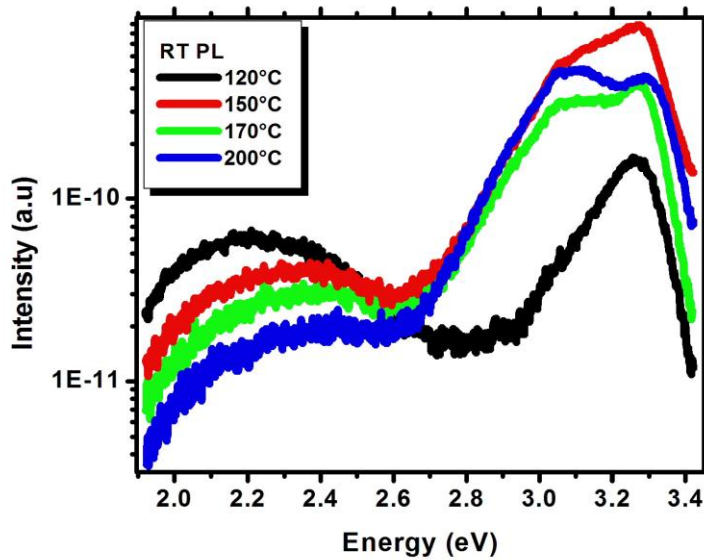
Figure 14: PL spectra of the studied samples measured at room temperature (RT).
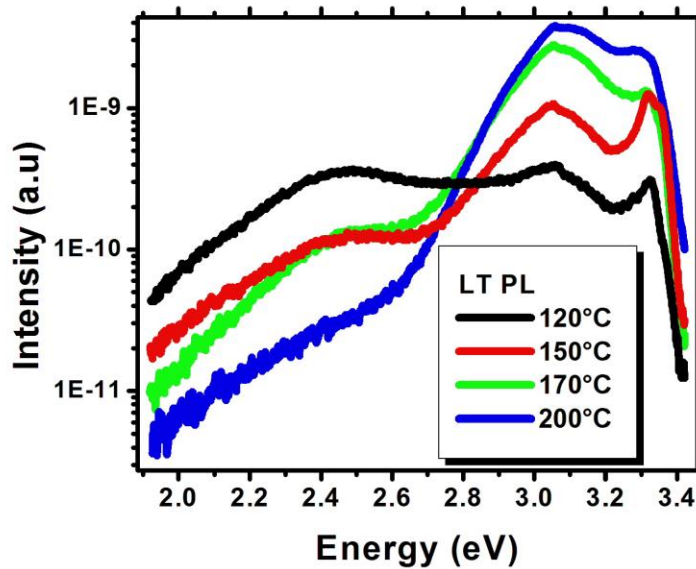
Figure 15: PL spectra of the studied samples measured at low temperature (LT).

SPV

SPV characterization of all the samples was performed in either nitrogen gas or vacuum environment. Ohmic contacts were made on top of the ZnO surface with indium and were connected to the sample holder by a vacuum-compatible carbon tape.

SPV spectra results

SPV spectroscopy was performed in all the samples to determine the bandgap, conductivity type, and the gap states in the surface as well as in the buried interface. In an *n*-type semiconductor band are bent upward toward the surface. During the super-bandgap illumination the band bending decreases, resulting in the positive SPV (negative CPD) change for the *n*-type semiconductor [16, 18]. Thus, SPV allows us to determine the conductivity type of the studied semiconductor. Our SPV spectral data of the ZnO thin films grown at different temperatures (see figures 16-19) indicate that they all are of an *n*-type.

The shown SPV spectra were measured in the nitrogen environment. We were not able to obtain meaningful spectra in vacuum, the reason for which is being investigated. The samples grown at 150°C, 170°C, and 200°C show a rather pronounced *n*-type band gap transition at ~ 3.2 eV (the change of the slope at ~ 2.0 eV is not an actual electronic transition but an artifact of a transition from one filter to another), while for the sample grown at 120°C this transition is very weak. Apart from the weak bandgap transition, the sample grown at 120°C showed several other SPV transitions not present in other samples: at ~ 1.2 eV (from a gap state to the conduction band), ~ 1.4 eV, and ~ 1.8 eV (both from the valance band to gap states). We believe that these transitions, because of the qualitatively different outlook of the entire spectral region, could be associated not with the ZnO film but with the states present at the ZnO buried interface with Si. Later in this text we will provide additional arguments in favor of our hypothesis. The weak bandgap transition for the sample grown at 120°C is due to the lower quality of the thin film, consistent with both the PL and AFM results mentioned above. In the samples grown at the higher temperatures one can see the change of slope at ~ 2.0 eV but this is not the actual transition but the filter artifact. The shown SPV spectra were measured in the nitrogen environment. We were not able to obtain meaningful spectra in vacuum, the reason for which is being investigated.
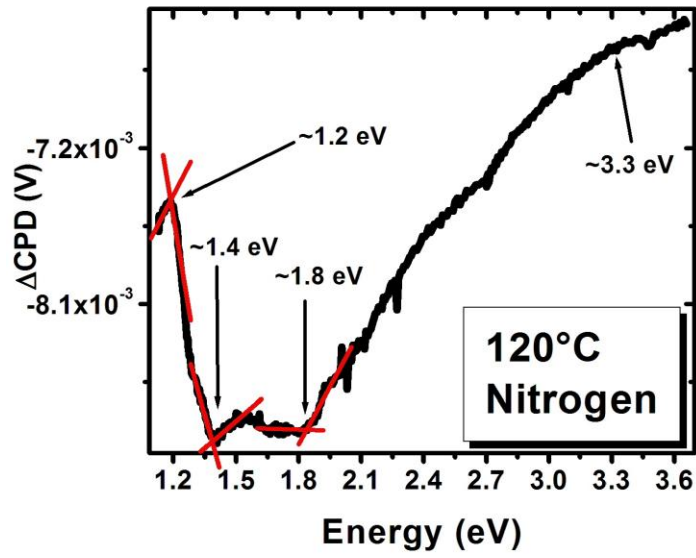
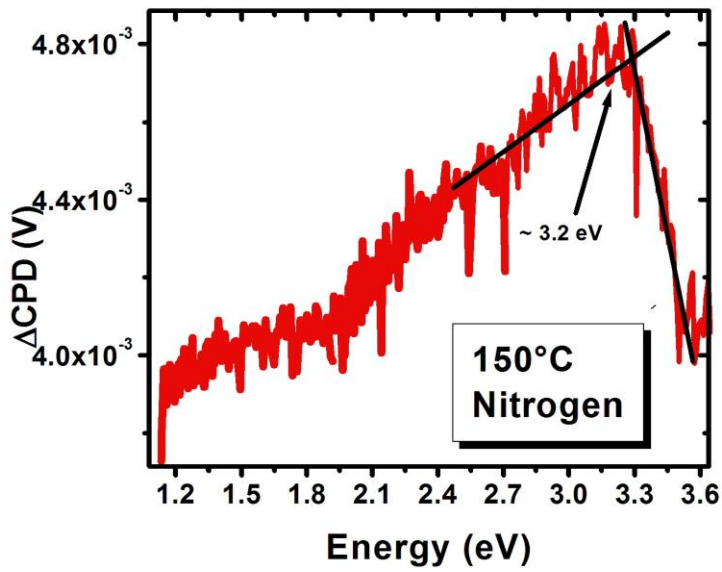Figure 16: SPV Spectra of ZnO film grown at 120°C.

Figure 17: SPV Spectra of ZnO film grown at 150°C.
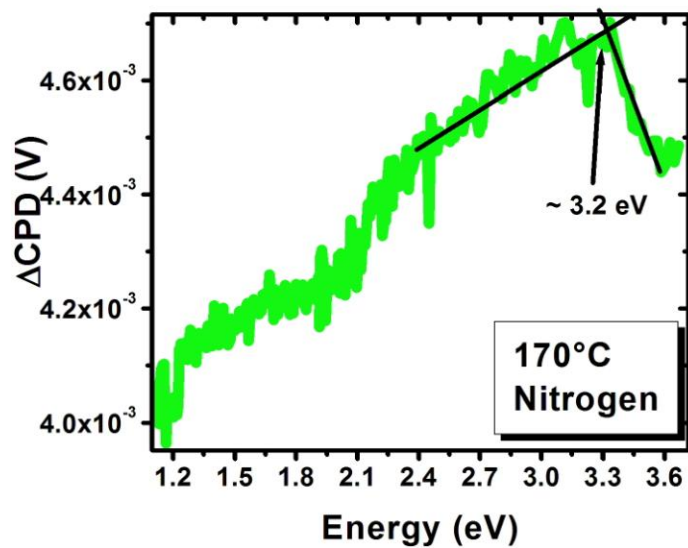
Figure 18: SPV Spectra of ZnO film grown at 170°C.
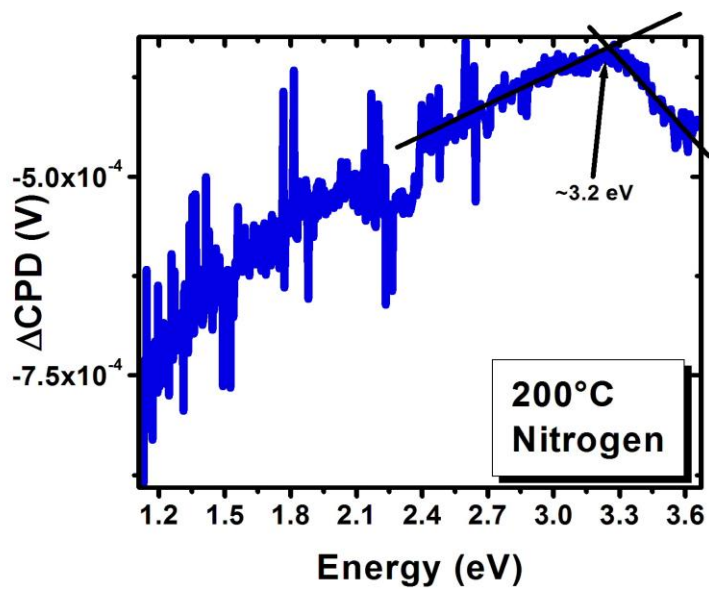
Figure 19: SPV Spectra of ZnO film grown at 200°C.

Transient SPV

Transient SPV measurements were performed in the nitrogen and vacuum to investigate the influence of buried interfaces on the charge dynamics in ZnO thin films grown on Si substrates. In order to obtain transient SPV the CPD change is monitored as a function of time consecutively under super-bandgap illumination and in the dark. An example of an SPV transient for both the light-on and light-off intervals on the linear time scale is shown in figure 20(a). These transients could be approximated rather well with simple (trivial) time exponential dependencies. Figure 20(b) shows the light-off part of a similar transient on logarithmic time scale.

In some measurements, however, transient curves exhibit more complex shapes, which could be better seen when plotted on the logarithmic time scale – cf. figures 20(b) and 20(c). In such case, the transient dependencies could be fitted by a superposition of several exponential dependencies with different characteristic times. For example, the transient curve obtained during the light-off process shown in figure 20(c) reveals two processes with different time constants. The presence of fast and slow components might indicate, e.g., a complex electronic bandgap structure for which more than one type of charge recombination phenomena contributes to the transient behavior.
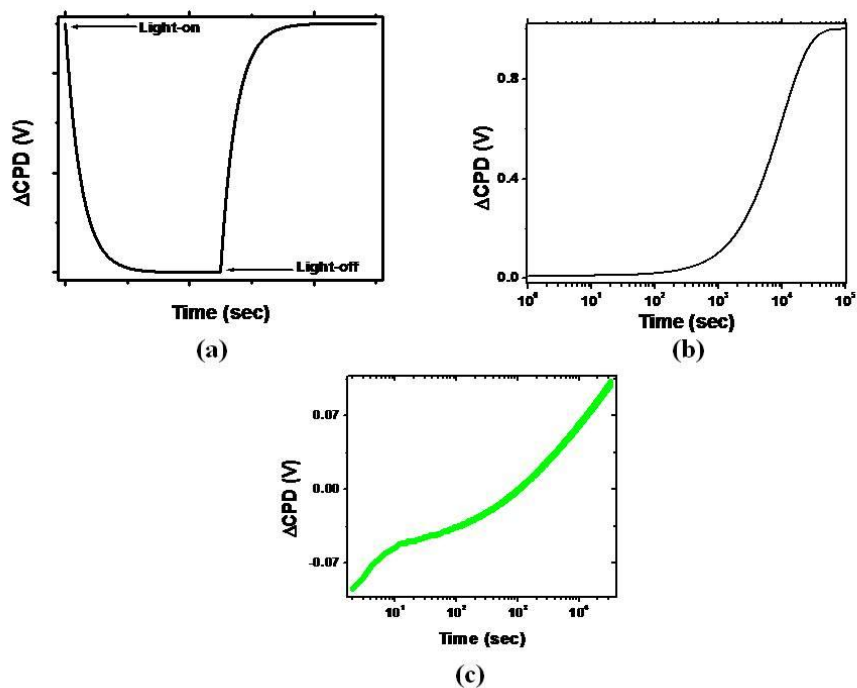
Figure 20: (a) Example of light-on and light-off SPV transients with a trivial exponential dependence plotted on a linear time scale, (b) Example of a light-off SPV transient with a trivial exponential dependence plotted on a log of time scale, (c) Example of a light-off SPV transient with multiple components plotted on a log time scale.

The studied samples were illuminated with white light in the nitrogen gas and vacuum environments to obtain the light-on and light-off SPV transients. In all the experiments, during the light-on intervals the CPD decreased, indicating a decrease in the band bending while during the light-off intervals the CPD increased. An example of a transient SPV curve on a linear time scale for the sample grown at 200°C is shown in figure 21. However, as discussed above, informative analysis of SPV transients should be performed employing the logarithmic time scale in order to elucidate possible multiple charge recombination mechanisms.
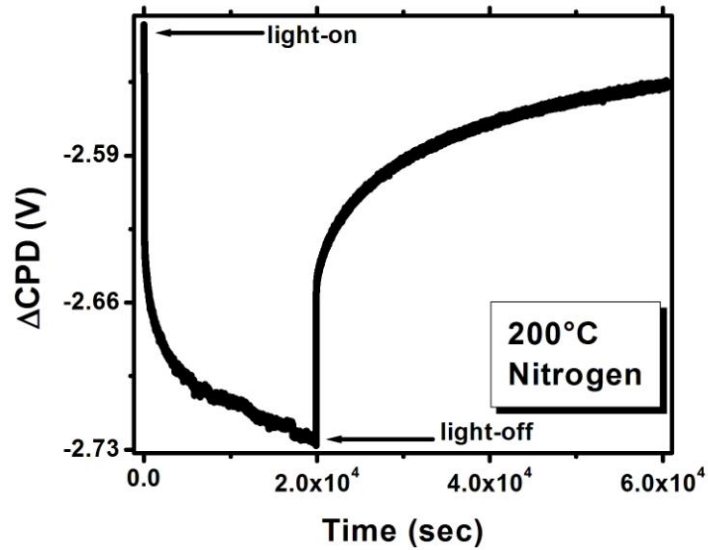
Figure 21: Transient SPV curve obtained in nitrogen gas environment for the sample grown at 200°C.

Figures 22-25 show the light-off transients on the logarithmic time scale collected in vacuum and in nitrogen gas for all the samples studied. For all the samples the light-off transient curves collected in the nitrogen gas environment reveal multiple processes occurring with different characteristic times. In vacuum, only the sample grown at 120°C showed both the fast and the slow processes whereas other samples exhibited only the relatively fast component. The characteristic time of the fast processes seems to be of the order of a few seconds (up to ~10 seconds) and the slow process occurs over a period of many hours. For the sample grown at 120°C the characteristic time of the fast process in the nitrogen gas environment is much shorter than for other samples. Also the relative intensity of the CPD change occurring for the fast process is much greater for the sample grown at 120°C than for other samples. The reasons for this will be discussed later in the text.

31
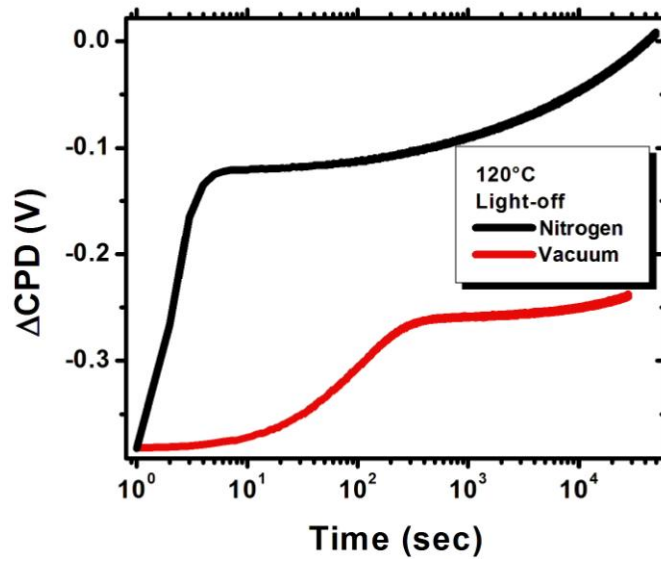
Figure 22: Light-off SPV transients on the log time scale for the ZnO thin film grown at 120°C.
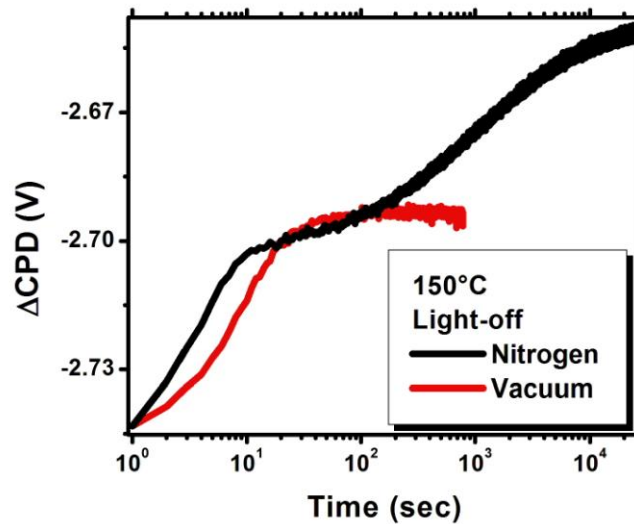
Figure 23: Light-off SPV transients on the log time scale for the ZnO thin film grown at 150°C.
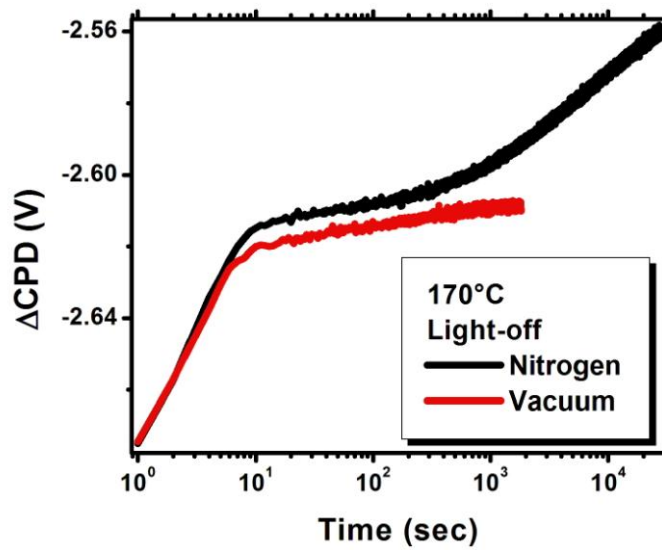
Figure 24: Light-off SPV transients on the log time scale for the ZnO thin film grown at 170°C.
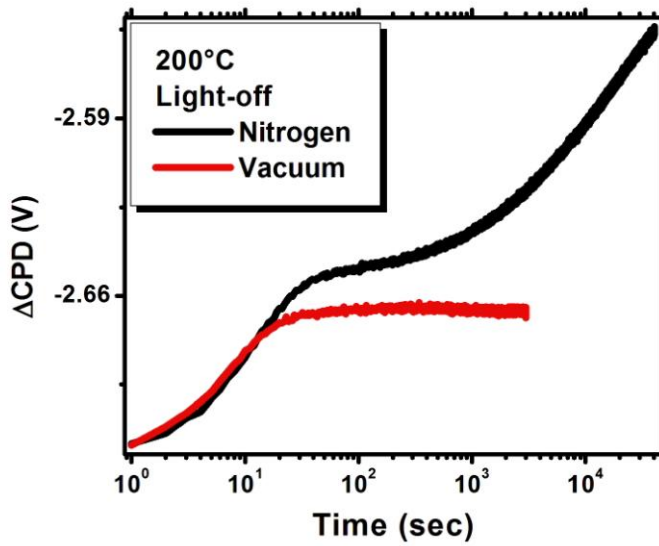
Figure 25: Light-off SPV transients on the log time scale for the ZnO thin film grown at 200°C.

Since the samples are thin films of ZnO grown on Si substrates, the transient curves may exhibit dominating contributions from either the buried interface (figure 26(a)) or the free surface (Figure 26(b)).
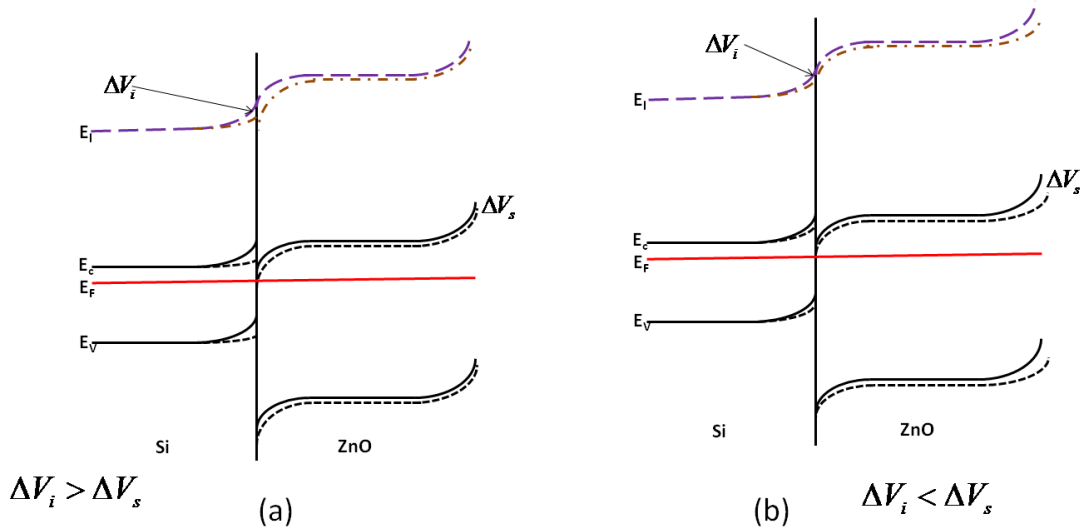
Figure 26: Band alignment diagrams for the ZnO/Si system with the dominating contribution to the SPV signal (a) from the free ZnO surface (b) from the ZnO/Si interface. Solid lines indicate the light-off intervals and the dotted lines – the light-on intervals.

During the light-off process the electrons in the conduction band can overcome, due to thermal excitations, the barrier at the free surface of ZnO or buried interface with Si and become trapped by the gap states present at the free surface or at the buried interface. Since the light-off process is activated only thermally, the time for the electrons to overcome the barrier and then become captured by the states close to the conduction band edge is relatively shorter than the time it will take for these electrons to be captured by the gap states which are

farther away from the conduction band. Thereby it is possible that the observed fast process may be associated with the electrons from the conduction band of Si overcoming the barrier and being trapped at the buried interface states close to the conduction band edge, whereas the slow process may be due to the electrons being trapped at the defects states that are far from the conduction band, at both the free surface and the buried interface. Another possible mechanism for the slow processes may be associated with the adsorbed species on the free surface of ZnO. It is likely that the interface band bending is dominating in the sample grown at 120°C (figure 26(a)), whereas for the rest of the samples the free surface band bending dominates, as in figure 26(b). For the former, the barrier height for the electrons in the interface region is largely reduced compared to other samples. It has been reported that for the n-ZnO/n-Si interface there are trap states at $E_c - 0.08$ eV [22]. The shorter times for the fast process observed in the sample grown at 120°C may be associated with the existence of such states at the buried interface that are very close to the bottom of the conduction band. Since the change in the band bending at the interface is greater in the sample grown at 120°C there are large numbers of electrons overcoming the barrier and getting trapped at the gap states, and thus the relative intensity of the fast process is significantly greater in this sample. On the other hand, it is likely that for the samples grown at higher temperatures, the concentration of defect states close to the bottom of the conduction band is much lower, because of the higher sample quality. Thus, the fast process takes a longer time in those samples. Moreover, in the SPV transients for these samples obtained in a gas environment, the dominating contribution for the slower states comes probably from the species adsorbed at the free interface. During evacuation of the chamber these adsorbed species may get desorbed from the surface of ZnO, and thus only the fast SPV components are observed in

those samples. On the other hand, the multiple SPV transient processes observed in vacuum for the sample grown at 120°C may be due to the electrons trapped at the deep states associated with the buried interface.

Conclusions

Using PL and SPV we studied ZnO thin films ALD-grown at four different temperatures on Si substrates. The SPV transients of these films are affected by the sample growth temperature and are quite sensitive to the experimental environment. All the samples showed multiple transient components during the light-off measurements in the nitrogen gas environment, while in vacuum (except for the sample grown at 120°C) they showed only the fast component. We provide a model explaining the observed transients. In particular, the charge recombination dynamics in the sample grown at 120°C is dominated mostly by the buried interface with the Si substrate. These results are consistent with the measurements performed using AFM, RT and LT PL as well as SPV spectroscopy.

Future work

We have found that charge dynamics of oxide semiconductor such as ZnO thin films grown on Si is influenced by the buried interfaces. Thus, in the future we would like to investigate the influence of buried interfaces on the titanium dioxide (TiO_2) thin films grown on Si by the sol-gel spin-coating method. TiO_2 has been extensively investigated for, among many others, photocatalytic applications. Reportedly, the photocatalytic activity of TiO_2 strongly depends on the preparation methods and post growth treatment conditions such as, e.g., calcination temperature [23]. Among various factors such as calcination temperatures, growth methods that influence the photocatalytic activity the key is the electronic structure of the TiO_2 itself [23]. For example, as has been shown earlier by our group, electronic structure of TiO_2 modified by silver revealed formation of extra states within the bandgap likely responsible for the increased photocatalytic activity of the silver-doped system [19]. However, modification of the electronic structure due to the calcination temperatures is often overlooked while studying the photocatalytic activity of thin film titanium dioxide. Calcination temperatures are often employed to control the thin films quality (including the quality of the interface), which is crucial for photocatalytic applications [23]. Thus, we will focus our interest on the effects of calcination temperatures on the electronic properties of the interface. TiO_2 is generally perceptive to the ambients and therefore is used in low-cost gas sensors with high sensitivity and fast response, thus our interest in the influence of the surface adsorbates on the charge transport properties in the investigated titania samples.

Titanium dioxide (TiO$_2$)

Another oxide system studied here is titanium dioxide. TiO$_2$ crystalizes mostly into three polymorphs: rutile, anatase, and brookite. Rutile and anatase structures are more stable thermodynamically [24]. Anatase ,rutile, brookite have a bandgap of ~ 3.2 eV , ~ 3.0 eV, and ~ 3.1 eV respectively [24]. In TiO$_2$, bonding between Ti and O is mixed ionic and covalent. The valance band is formed by the 2p states of oxygen and the conduction band – by the 3d states of titanium.

TiO$_2$ is a material of choice for photocatalytic (PC) applications. PC reaction occurs as a result of the electron-hole pair separation due to radiation. The separated charge carriers participate in the decomposition of the surface absorbent. Since TiO$_2$ has a wide bandgap, the charge separation occurs only when ultraviolet (UV) light is used. Solar light consists of mainly 43% of visible light and only 5% of UV light [25]. Visible light PC activity of the TiO$_2$ is achieved only when there are states within the bandgap that can absorb the visible light. It is well known that native defects such as oxygen vacancies may induce energy levels within the bandgap which can play an important role in visible light PC activity. These defects can be created during growth and post growth processing of TiO$_2$.

A number of methods have been reported to prepare TiO$_2$ thin films including, atomic layer deposition [26], chemical vapor deposition [27], and sol-gel process [28]. The sol-gel method offers many advantages over other deposition techniques such as simplicity, low cost of the equipment used, low temperature budgets, and ease of large area coating. The quality of TiO$_2$ thin films depends on the various growth factors such as the ratio of precursors used, film thickness, and calcination temperatures. For example, in [28] the authors studied the roles of solvent and calcination temperatures. They found that the TiO$_2$ with greater amounts

of solvent and multiple coating cycles resulted in thin films of higher quality. The calcination temperatures can change the structure of TiO_2 from amorphous to anatase or rutile [23, 28]. The sol-gel grown TiO_2 films calcined above 400°C are of the anatase structure whereas for some other methods such as liquid phase deposition method the anatase phase is obtained only when calcined at 500°C. Thus, it is important to understand the correlation between the growth methods as well as processing temperatures on the structure of TiO_2 films.

For the different applications of the TiO_2 high quality thin films are required where the crucial role could be played by the buried interfaces. The mechanisms of charge transfer are of interest for the increased performance of, for example solar cells, photocatalytic devices, etc. Defects at the interface may play the role of charge recombination centers, which could be beneficial or detrimental in applications. Thus, it is desirable to probe the electronic structure at the buried interfaces of TiO_2 thin films. As of today there is a rather limited amount of work performed in this area.

The calcination temperatures of TiO_2 affect the photocatalytic (PC) activity, which is higher in the anatase phase than in rutile. Among other factors impacting PC activity are the value of the bandgap energy, as well as the concentration and energetics of the states within the bandgap. For example, it has been shown by our group that a silver-modified TiO_2 reveals extra states induced in the bandgap. The calcination temperatures may also introduce new or modify existing states within the bandgap which could influence the PC activity [23]. In this work, we investigate the effects of the calcination temperatures on the electronic structure of the free surface and buried interfaces in TiO_2 thin films calcined at various temperatures.

The adsorption or desorption of atomic, radical and molecular species at semiconductor surfaces often induces charge transfer between the surface and the bulk resulting in near-surface band bending. Rothschild et al., studied the role of chemisorbed oxygen on titania thin films by SPV [29]. It was shown that the band bending increases with oxygen exposure. In [30] it was found that while in dry nitrogen gas environment anatase and rutile TiO_2 display an n-type behavior, under wet conditions the surface conductivity type converts to a p-type. Onda et al., demonstrated that for the modified TiO_2 surfaces oxygen acts as an acceptor on surface defect states whereas water acts as a donor molecule [31]. These and other examples demonstrate how crucial it is to understand the impact of adsorption and desorption on the electronic transport properties in TiO_2 thin films, including charge transport mediated by buried interfaces.

TiO$_2$ sample preparation

As we mentioned above, TiO_2 thin films can be obtained by the sol-gel spin-coating method, which is inexpensive and requires low growth temperatures.

The precursors used to prepare the TiO_2 sol are titanium n-butoxide, nitric acid, ethanol and deionized water. 5.03 g of ethanol and 5.3 g of titanium n-butoxide were mixed and mechanically stirred. In another beaker 0.562 g water was measured and 4.31 g of nitric acid was added. The resulting mixture was then added to 5.03 g of ethanol. The mixture of water, nitric acid and ethanol was added drop-wise to the titanium n-butoxide and ethanol solution. The prepared mixture was stirred for another 24 hours. The obtained sol was then spin-coated onto silicon substrates to obtain thin films. The films were dried in air for 30 minutes and then heated at around ~ 80°C for about 30 minutes with a subsequent cool-down

at room temperature. The obtained films were calcined in air at different temperatures for ~

4 hours. The samples were then characterized to determine the structure. The schematic

flow chart of the growth procedure is shown in figure 27.
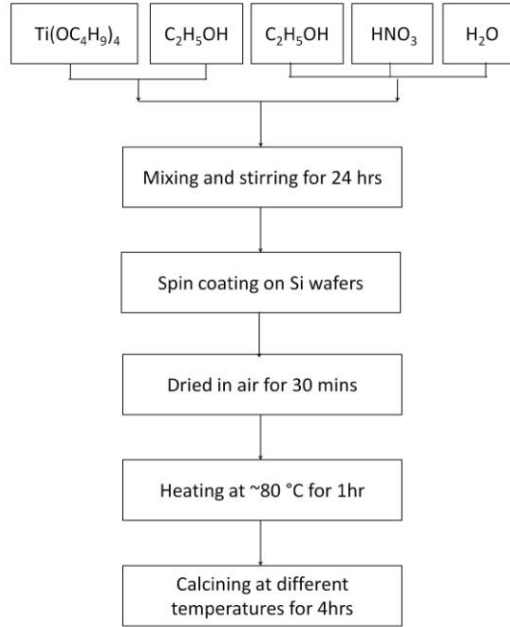
Figure 27: Flow chart illustrating preparation steps of the studied titania thin film samples.

Raman spectroscopy

The inelastic scattering of light is called the Raman effect. When a beam of light is

incident on a sample, photons are absorbed by the material and then scattered. Most of the

scattered photons have exactly the same wavelength as the incident photons (Rayleigh

scattering). However, a small fraction of the scattered radiation is shifted to a different

wavelength due to Raman scattering. We used 200A NIR 532 with excitation wavelength

785 nm to get Raman spectra.

TiO$_2$ results

The structure of the TiO$_2$ thin films grown by the sol-gel method and then calcined at 500°C, 600°C and 700°C were investigated by Raman spectroscopy. Raman spectra for these samples are shown in figure 28.
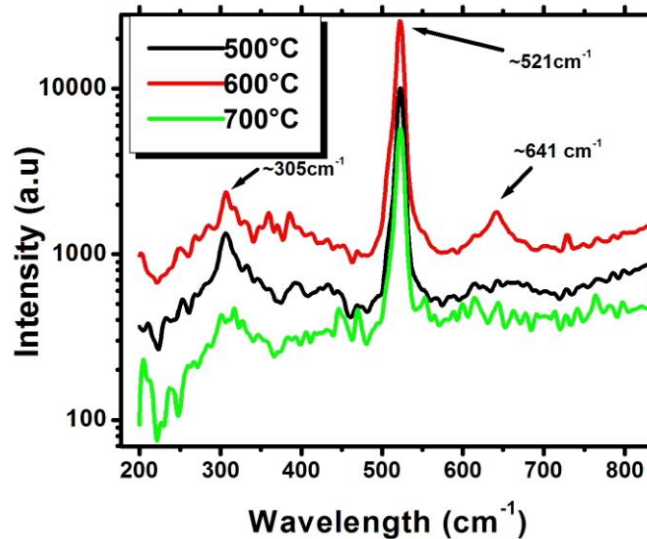

Figure 28: Raman spectra of TiO2 sol-gel grown thin films calcined at various temperatures.

In the literature the Raman active lattice vibration for anatase phase has been assigned at 143.4 cm^{-1} (E_g), 196.2 cm^{-1} (E_g), 396.5 cm^{-1} (B_{1g}), 517.7 cm^{-1} ($A_{1g} + B_{1g}$), and 639.4 cm^{-1} (E_g), [31] whereas the rutile phase – to the four Raman modes at 143 cm^{-1} (B_{1g}), 447 cm^{-1} (E_g), 612 cm^{-1} (A_{1g}), and 826 cm^{-1} (B_{2g}) [32]. In our measurements, we observed peaks at 305 cm^{-1} and 521 cm^{-1} due to the silicon substrate for all the samples calcined at different temperatures. However, for the sample calcined at 600°C an extra peak at ~ 641cm^{-1} appears, most likely due to the anatase phase. This result is quite stimulating for our future work.

References

1. R. Ramesh and D.G Schlom, *MRS Bulletin* **33**, (2008).

2. D.Cammi and C. Ronning, *Advances in Condense Matter Physics*, **2014**, 184120, (2014)

3. M. A. Gluba, N. H. Nickel, K. Hinrichs, and J. Rappich, *J. Appl. Phys.*, **113**, 043502 (2013).

4. J. L. Pau, J. Piqueras, D. J. Rogers,F. Hosseini Teherani, K. Minder, R. McClintock, and M. Razeghi, J Appl phys, **107**, 033719, (2010).

5. K. Liu, M. Sakurai, and M Aono, *Sensors* **10***,* 8604 (2010).

6. J. D. Ye, S. L. Gu, S. M. Zhu, W. Liu, R. Zhang, Y. Shi, Y.D. Zheng, *Appl. Phys. Lett* ,**88**, 182112 (2006).

7. J. C. Moore, and C. V. Thompson, *Sensors* **13***,* 9921-9940, (2013).

8. W. Li, C. W. Wu, W.G. Qin, G.C. Wang, S. Q. Lu, X. J. Dong, H. B. Dong, Q. L. Sun, *Physica B*, **404**, 2197-2201, (2009).

9. U. Ozgur, Ya. I. Alivov, C. Liu, A. Teke, M. A. Reshchikov, S. Dogan, V. Avrutin, S.-J. Cho, and H. Morkocd, *J. Appl. Phys*. **98**, 041301, (2005).

10. V. De Walle, C.G. *Phys. Rev. Lett.* **2000**, *85*, 1012 – 1015

11. D. Saha, Amit. K. Das, R. S. Ajimsha, P. Misra, and L. M. Kukreja, *J. Appl. Phys.*, **114**, 043703 (2013).

12. E. Guziewicz, I. A. Kowalik,1 M. Godlewski, K. Kopalko, V. Osinniy, A. Wojcik,

S. Yatsunenko, E. Lusakowska, W. Paszkowicz, and M. Guziewicz, *J. Appl. Phys*., **103**, 033515 (2008).

13. E Przezdziecka , L Wachnicki1, W Paszkowicz, E Łusakowska, T Krajewski, G Luka1, E Guziewicz, and M Godlewski, *Semicond. Sci. Technol*., **24**, 105014 (2009).

14. Y. Lin, D. Wang, Q. Zhao, Z. Li, Y. Ma, M. Yang, *Nanotechnology*, 17, 2110-2115 (2006)

15. R. Gurwitz, R. Cohen, and I. Shalish, *J. Appl. Phys,***115** 033701 (2014)

16. L. Kronik and Y. Shapira, *Surf. Sci. Rep*., **3**, 1 (1999).

17. R. M. Peters, Phd thesis, **TCU**, 2010.

18 L. Kronik and Y. Shapira, *Surf. Interface Anal*., **31**: 954–965 (2001).

19 A. Nemashakalo, PhD thesis, TCU, 2014

20. D. Gal, J. Beier, E. Moons, G. Hodes, D. Cahen, L. Kronik, L. Burstein, B. Mishori, M. Leibovitch, Y. Shapira, D.Hariskos, R. Klenk, H.-W. Schock, *Proc. AIP.*, **353** (1995).

21. C. H. Chan, J. D. Wu, Y. S. Huang, Y. K. Su, and K. K. Tiong, *J Appl Phys*., **106**, 043523 (2009).

22. V. Quemener, M. Alnes, L. Vines, O. Nilsen, H. Fjellvag, E.V. Monakhov, and B.G. Sevensson, *Solid State Phenomena*, **178-179**, 130-135, (2011).

23. J.-G. Yu, H.-G. Yu, B. Cheng, X.-J. Zhao, J. C. Yu, and W. K. Ho, *J Phys Chem. B.*, **107**, 13871 (2003)

24. U. Diebold, Surf. Sci. Rep, **48**, 53 (2009).

25. S.G. Kumar and L. G. Devi, *J Phys. Chem A.*, **115**, 13211(2011).

26. M. Reiners, K. Xu, N. Aslam, A. Devi, R. Waser, and S. Hoffmann-Eifert, *Chem Mater*, **25**, 2934 (2013).

27. S. Mathur, P. Kuhn, *Surface & Coatings Technology*, **201**, 807–814 (2006).

28. P. Kajitvichyanukula, J. Ananpattarachaia, S. Pongpomb, *Science and Technology of Advanced Materials*, **6**, 352–358, (2005).

29. A. Rothschild, A. Levakov, Y. Shapira, N. Ashkenasy, Y. Komem , *Surf. Sci.*,**532-535**, 456, (2003).

30. D. S. Warren, Y. Shapira, H Kisch, and A. J. McQuillan, *J Phys Chem C.*, **111**, 14289, (2007).

31. K. Onda, B. Li, H. Petek, *Phys Rev B.*, **70**, 045415 (2004).

31. H. C. Choi, Y. M. Jung, and S. B. Kim Bull, *Korean Chem. Soc.,***25**, 426, (2004).

32. V. Swamy, and B. C. Muddle, *Appl. Phys Lett.*, **89**, 163118 (2006).

VITA

Personal Background   Shreedhar Nath Pant

Kathmandu, Nepal.

Married, No Child

Education: Master in Physics,

Tribhuvan University, Kathmandu, Nepal, 2006.

Master in Physics,Texas Christian University,

Fort Worth, 2015

Experience: Teaching Assistant, Texas Christian University

2010-2015

Abstract

INFLUENCE OF BURIED INTERFACES ON THE CHARGE DYNAMICS IN OXIDE THIN FILMS

By Shreedhar Nath Pant, 2015

Department of Physics and Astronomy

Texas Christian University

Thesis Advisor: Dr. Yuri M. Strzhemechny –Associate Professor of Physics

Influence of buried interfaces was investigated in the ZnO thin films grown on Si at 120°C, 150°C, 170°C, and 200°C. by employing PL and SPV. The PL spectrum of samples grown at higher temperatures showed bandgap emission at ~3.3 eV, shallow defects emission ~3.0 eV and visible emission at ~2.4 eV. On the other hand, the visible emission for the sample grown at 120°C visible emission is red-shifted to ~2.1eV. SPV spectra of films grown at higher temperatures in nitrogen gas showed bandgap transition whereas 120°C grown sample only showed weak band transition. Instead one can see transition primarily in IR region due to silicon or silicon oxide. Furthermore, analysis of the transient SPV curves in both nitrogen and vacuum revealed two different characteristic time scales (fast and slow) possibly reflecting contributions of both the ZnO surface and the ZnO/Si buried interface.